

# Diagnostics of the oceanic thermohaline circulation in a coupled climate model

Rainer Bleck<sup>a,\*</sup>, Shan Sun<sup>b</sup>

<sup>a</sup>*Los Alamos National Laboratory, Mail Stop B296, Los Alamos, NM 87545, USA*

<sup>b</sup>*Goddard Institute for Space Studies, New York, NY 10025, USA*

Received 14 May 2002; accepted 17 April 2003

## Abstract

Two century-scale integrations of a global coupled model consisting of the GISS atmospheric model and the HYCOM ocean model are carried out: a control run assuming fixed atmospheric composition, and a perturbation run assuming gradual doubling of CO<sub>2</sub>. The model does not use flux corrections at the air–sea interface, nor is the ocean “spun up” prior to coupling. When increasing CO<sub>2</sub> at the rate of 1% per year to twice its original level and keeping it constant thereafter, the model responds with a 2 °C increase in 200 years in the global mean surface air temperature and a virtually unchanged Atlantic meridional overturning circulation (MOC). Due to the predominantly isopycnic character of HYCOM, geographic details of the 3-D thermohaline circulation in potential density space can be extracted from the model output with relative ease. The analysis confirms that even regional details of the MOC in this experiment are rather insensitive to the climate change brought on by CO<sub>2</sub> doubling. Furthermore, the analysis reveals strong similarities between the simulated and the observed MOC.

© 2003 Elsevier B.V. All rights reserved.

**Keywords:** Oceanic thermohaline circulation; Climate model; HYCOM

## 1. Introduction

The need to distinguish natural variability from manmade trends in the earth’s climate system provides a driving force for the development not only of coupled atmosphere–ocean–land models, but also of tools useful for diagnosing a plethora of interaction modes in the coupled system. One particularly striking example of an interaction is the possible slowdown of the Atlantic branch of the oceanic meridional

overturning circulation (MOC) during global warming. Such a slowdown is projected by most of today’s climate models according to results compiled in [Fig. 9.21 of IPCC \(2001\)](#).

[Sun and Bleck \(2001b\)](#) recently reported on coupled simulations carried out with the GISS atmospheric model and a hybrid-isopycnic coordinate ocean model called HYCOM ([Bleck, 2002](#)). In their simulation, the Atlantic MOC maintains its strength as atmospheric CO<sub>2</sub> concentration gradually increases at the rate of 1% per year to twice its initial value, remaining constant thereafter. The present article illustrates an attempt to search for possible changes in the geographic layout of the MOC that may have

\* Corresponding author. Fax: +1-505-667-5921.

E-mail address: [bleck@lanl.gov](mailto:bleck@lanl.gov) (R. Bleck).

happened in the model during CO<sub>2</sub> doubling, using analysis techniques originally presented in Sun and Bleck (2001a).

## 2. Experimental setup

The atmospheric module employed in the coupled runs is the SI2000 GISS atmospheric model (Hansen et al., 2002), based on model SI95 with finer vertical resolution and improved physics packages (Hansen et al., 1997). It has 12 levels in the vertical and a  $4 \times 5^\circ$  spherical grid in the horizontal.

The oceanic component HYCOM uses  $\sigma_2$  (potential density, referenced to 2000 m, minus  $1000 \text{ kg m}^{-3}$ ) as vertical coordinate in the oceanic interior. Coordinate layers in this model level off to become constant-depth layers wherever the isopycnals they follow outcrop at the sea surface. Thermobaric effects (Sun et al., 1999) are included. The bottom topography is obtained by spatially integrating ETOPO5 data of  $5'$  spatial reso-

lution over each grid cell. A Mercator mesh of resolution  $2^\circ \times 2^\circ \cos(\phi)$  is used south of latitude  $\phi' = 60^\circ \text{ N}$ . At  $\phi'$ , the Mercator projection smoothly transitions to a bipolar projection (Arfken, 1970, chapter 2.9) with poles over Canada and Siberia but without grid singularity over the ocean area as shown in Fig. 1. The Bering Strait is closed in this experiment. River runoff is incorporated by accumulating net freshwater input on each land point and directing it to prescribed river mouth locations where it is added as a point source to the precipitation field.

The ocean model is capped by the GISS 4-layer thermodynamic ice model (Russell et al., 2000). A relatively simple flux coupler employing zero-order interpolation transmits information about ocean-ice state variables to the atmospheric model which in turn computes surface fluxes. These fluxes are then interpolated back onto the ocean grid in a manner ensuring conservation of global flux integrals.

The two model runs start with atmospheric trace gases at 1951 levels, the oceanic climatology of

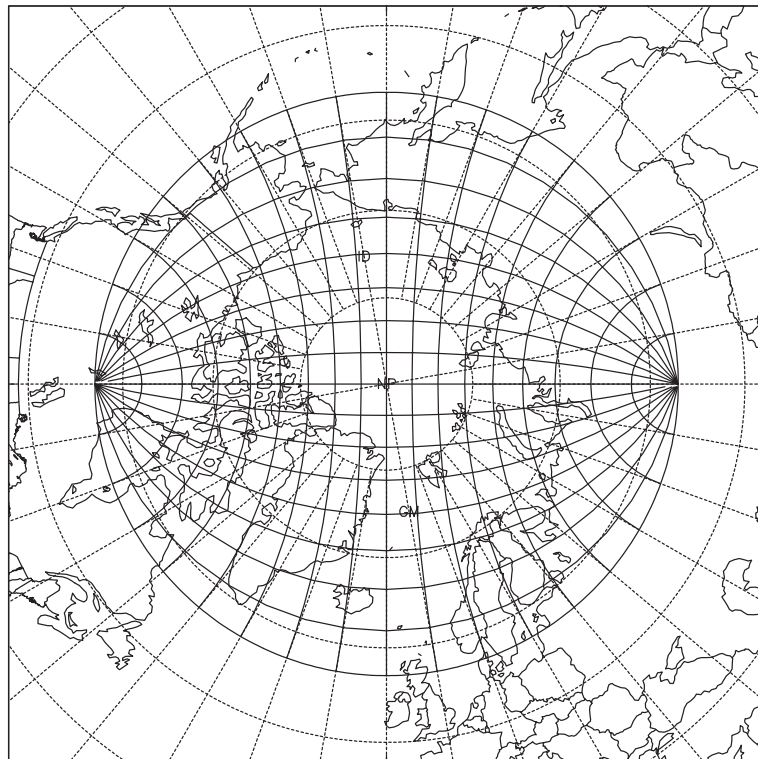


Fig. 1. The bipolar projection used in the model to represent the polar cap north of  $57^\circ \text{ N}$ . A Mercator projection is used south of  $57^\circ \text{ N}$ .

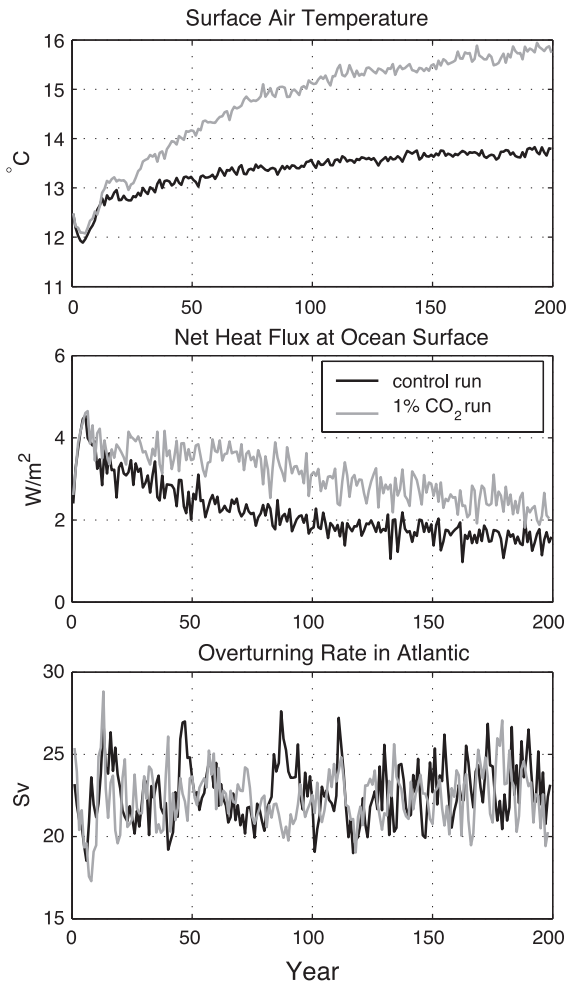


Fig. 2. Surface air temperature, net surface heat flux and Atlantic overturning stream function in the control and  $2 \times \text{CO}_2$  run.

Levitus et al. (1994), and the Hadley Centre ice climatology.

In the  $\text{CO}_2$  doubling experiment, the surface air temperature increases by  $2^\circ\text{C}$  in 200 years relative to the control run (Fig. 2, from Sun and Bleck, 2001b). The temperature is still climbing at the end of that period, as there is still a net heat flux of  $0.6 \text{ W/m}^2$  into the ocean at year 200 relative to the control run. The Atlantic overturning stream function appears to be stable in both runs, suggesting that it is insensitive to global warming resulting from gradual  $\text{CO}_2$  doubling, at least on a 200-year time scale.

In both runs, the amount of water in each isopycnal layer gradually drifts from its initial value based on Levitus climatology (Levitus et al., 1994). The drift is particularly large during the first 20 years (Fig. 3). Overall, the ocean is getting slightly warmer and saltier with time.

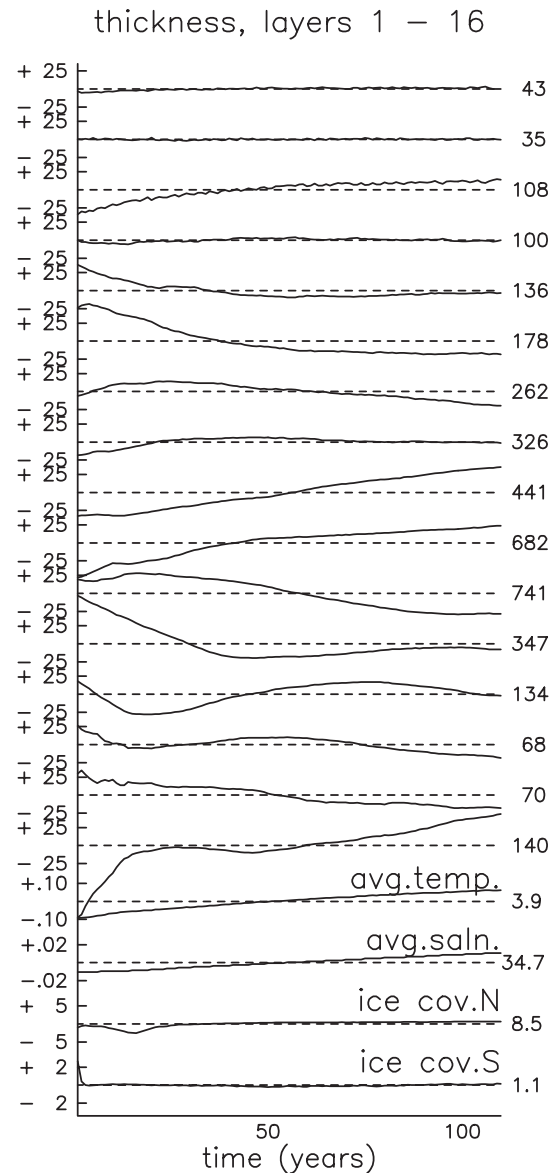


Fig. 3. Temporal variation of isopycnal layer thickness (m), global temperature ( $^\circ\text{C}$ ), salinity (psu), and ice coverage ( $10^6 \text{ km}^2$ ) in the control run. Long-term averages indicated on right.

### 3. Analysis method

Like other circulation models, HYCOM computes mass fluxes entering/exiting each of the six faces of individual grid cells; time integrals of these quantities are easily generated. In grid regions where coordinate surfaces in HYCOM follow isopycnals, the horizontal components of these mass fluxes represent the isopycnal (or adiabatic) component of the circulation while the vertical ones represent the diapycnal component. The latter component is usually small except in regions where the grid cell in question is “touched” at least intermittently by the surface mixed layer.

The six fluxes entering/exiting each grid cell represent a huge amount of information which needs to be reduced considerably before global or basin-scale circulation patterns emerge. The essential steps in the data reduction procedure, fully documented in [Sun and Bleck \(2001a\)](#), are the following:

1. Zonal/meridional isopycnal mass flux values are integrated over longitude/latitude segments, respectively, between points where the flux changes sign. In the case of a simple gyre circulation in a closed basin, for example, this procedure reduces the meridional and zonal mass fluxes across the pair of meridians and parallels intersecting at the gyre center to two positive and two negative—but otherwise equal—values representing the total northward, southward, eastward, and westward gyre transport. Rather than plotting each flux integral value halfway between the two points where the sign changes occur, we find it convenient to plot the flux integrals at flux-weighted locations.
2. Diapycnal mass flux values are grouped in the horizontal plane into clusters around significant maxima/minima. Fluxes in each cluster are summed up. This procedure is equivalent to determining the volume of a mountain from the elevation information presented on a standard topographic chart. As in the isopycnal flux reduction procedure just outlined, positive and negative flux values (representing “mountains” and “valleys”) are summed up separately to prevent cancellation. The result of this procedure is a finite set of mass flux values, each one representing the total upward or downward

interlayer transport in a geographically distinct region. The number of discrete flux values produced depends, of course, on which maxima/minima in the flux field is considered “significant.” However, the amount of tuning necessary to produce interpretable results has been found to be minimal.

The above procedures yield three maps, one for each component of the mass flux, which, if viewed together, yield a quantitative picture of the overall layout of the modeled three-dimensional circulation. The thermohaline-forced part of this circulation can be obtained, if needed, by identifying those parts of the isopycnal fluxes that clearly represent horizontal intra-basin recirculation systems, and subtracting them from the total flux values.

To remove possible ambiguities caused by the hybrid character of the coordinate layers in HYCOM, we initially transform all model-generated “raw” horizontal mass fluxes into isopycnal fluxes using the technique outlined in [Appendix D of Bleck \(2002\)](#). The corresponding diapycnal fluxes are deduced by mass conservation.

Results shown below are for the 20-year period centered on model year 100.

### 4. Results

Traditional diagnostics of the MOC typically consist of a stream function in depth-latitude coordinates indicating the strength of the overturning circulation in the world ocean or in individual ocean basins. An example of this type of diagnostics is given in [Fig. 4](#) for the control run. Note that the vertical coordinate in these plots is potential density anomaly  $\sigma_2$ . Therefore, the ocean surface appears tilted. Transforming mass fluxes to isopycnal space also has the effect of obliterating the distinction between horizontal and vertical circulations that can be made in a Cartesian reference frame. In other words, circulation systems that are horizontal in  $z$  space are depicted in density space, due to their thermal asymmetry (warm water moving poleward, cold water owing equator-ward), as vertical. This typically makes the overturning circulation appear stronger in density than in Cartesian space. A related facet is that thermally indirect circu-

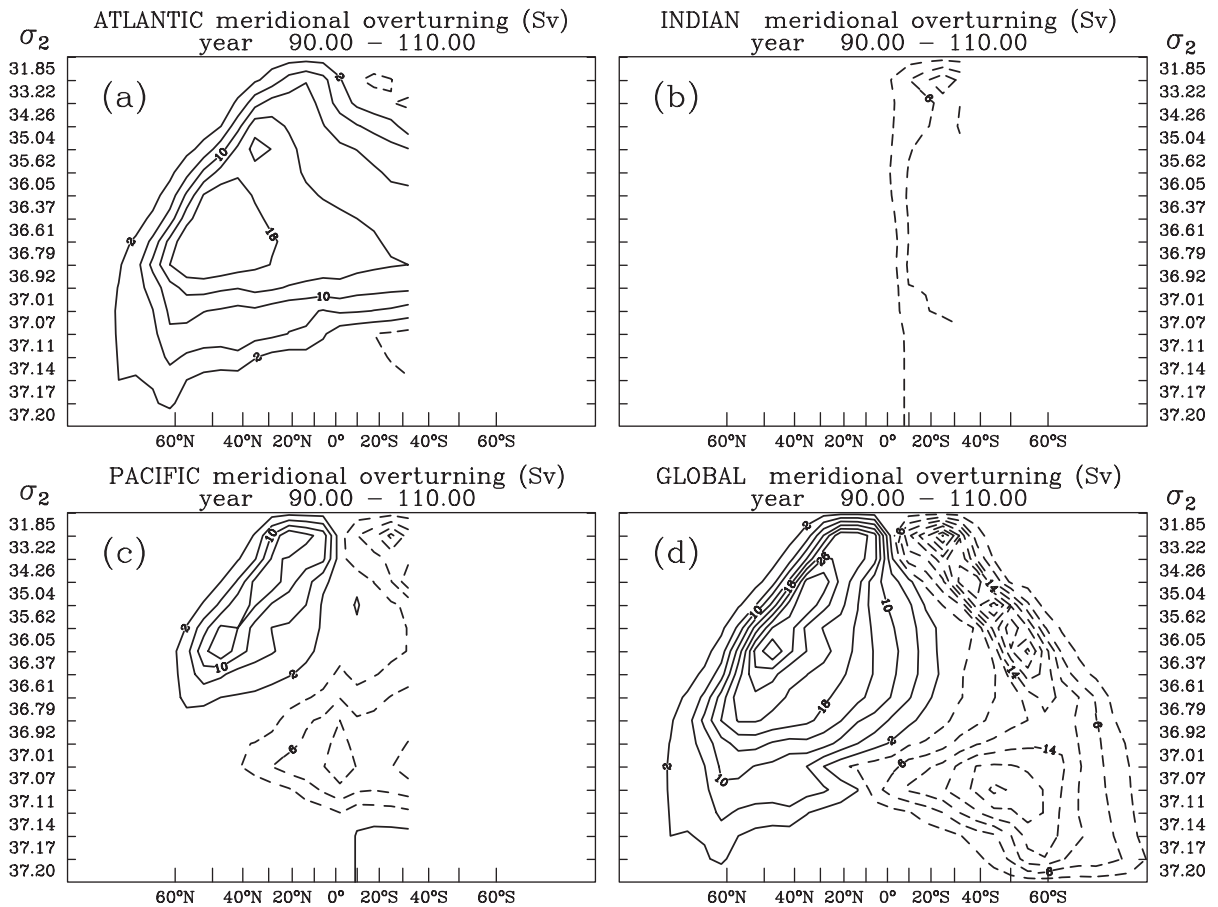


Fig. 4. Stream function ( $\text{Sv} \equiv 10^6 \text{ m}^3 \text{ s}^{-1}$ ) of the vertical-meridional overturning circulation in the control run, averaged over 20 years, in three ocean basins (a–c) and the world ocean as a whole (d). Dashed streamlines indicate clockwise motion. Abscissa: latitude ( $^\circ$ ). Ordinate:  $\sigma_2$ , defined as potential density anomaly referenced to 2000 m depth ( $\text{kg m}^{-3}$ ).

lation cells familiar from  $z$  or  $p$  coordinates, such as the atmospheric Ferrel cell and the oceanic Deacon cell, are eliminated by this transformation.

The rate of deep-water formation in the North Atlantic, roughly 20 Sv ( $1 \text{ Sv} \equiv 10^6 \text{ m}^3 \text{ s}^{-1}$ ) according to Fig. 4a, is compatible with observational estimates of  $18 \pm 4$  Sv from Macdonald (1998), but is higher than the 14 Sv obtained by Schmitz (2002). The rate of deep-water production in the North Pacific appears somewhat too strong. The global stream function (Fig. 4d) indicates a near-balance of deep-water production in the northern and southern hemisphere. The southern bottom water is slightly denser than the northern one, again in qualitative agreement with observations.

The meridional heat fluxes associated with the MOC are given in Fig. 5. These fluxes show the familiar north–south asymmetry and are in good agreement with available observational estimates (Macdonald, 1998, Trenberth and Caron, 2001) in other respects as well.

For the purpose of this article, the 16 model layers are lumped into two classes consisting of model layers 1–8 and 9–16, respectively. The zonal and meridional mass fluxes for the control run, obtained by the method outlined in the previous section, are displayed in Fig. 6 for the upper class and in Fig. 7 for the lower class. To assure readability, only the North Atlantic is shown. Readers studying the bands of arrows in detail soon will notice that zonal and meridional fluxes both

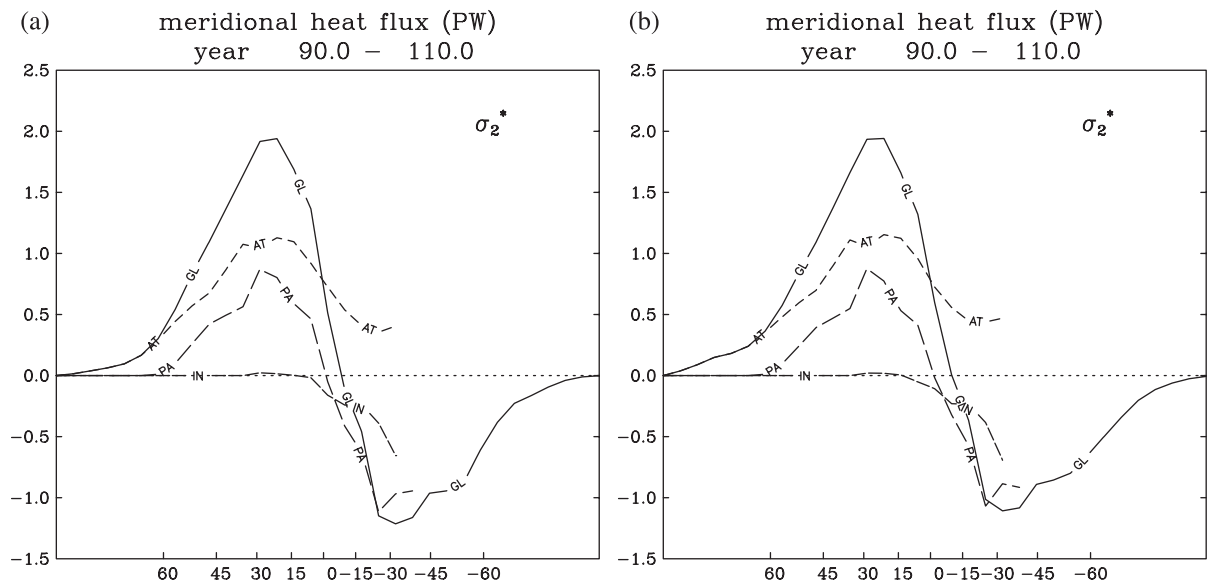


Fig. 5. Meridional heat flux ( $\text{PW} = 10^{15} \text{ W}$ ), averaged over 20 years, against latitude ( $^{\circ}$ ) in three ocean basins and the world ocean. (a) Control run; (b)  $2 \times \text{CO}_2$  run.

represent the total strength of an ocean current, rather than the  $x$  and  $y$  components of a flux vector.

One striking feature in the right panel of Fig. 6 is the large difference between northward and southward fluxes. An imbalance of opposite sign is seen in the right-side panel of Fig. 7. Both these imbalances are reconciled, of course, by the transfer of water between the upper and lower class. The geographic locations where this transfer takes place are delineated in the left panel of Fig. 8.

We see that the main sinking regions for North Atlantic water in the control run are the Davis Strait (with 4.1 Sv), the Denmark Strait (4.1 Sv) and the southern fringe of the Norwegian Sea (14.4 Sv). Taking into account the regions where the model produces weak upwelling, the net downward mass transport north of the 45th parallel comes to roughly 19 Sv, consistent with the maximum stream function value shown in Fig. 4a.

Schmitz (2002) divides the ocean into six vertical classes and estimates the Atlantic MOC in these classes based on hydrographic observations. We reproduce one of his results in Fig. 9. The dividing line between what Schmitz refers to as “intermediate” water and Upper North Atlantic Deep Water (UNADW) approximately corresponds to the dividing

line between our upper and lower class. This allows us to make quantitative comparisons of the model results with Schmitz’s estimates. We find that both circulation rate and path of the northward flow in the upper model class and the return flow in the lower model class match those in Schmitz (1996) and Fig. 9. The locations where the downward fluxes occur are also in fair agreement with observational evidence. Note in particular the correspondence between Schmitz’s estimate of 4 Sv of intermediate water being converted to UNADW in the Labrador Sea (see Fig. 9) and the 4 Sv of modeled conversion in the northern reaches of the Labrador Sea (left panel of Fig. 8).

In view of evidence presented in IPCC (2001), we had expected the Atlantic MOC to weaken in response to a doubling of atmospheric  $\text{CO}_2$ . However, the overturning stream functions diagnosed from the  $\text{CO}_2$  doubling run are found to be so similar to Fig. 4 that we will refrain from showing them here. (Differences are more noticeable 100 years later, at which time the NADW in the  $2 \times \text{CO}_2$  run is lighter by 1–2 model density classes compared to the control run.) The heat flux differences between the control and the  $\text{CO}_2$  doubling run are equally unremarkable. Proceeding to the next level of diagnostic detail, we



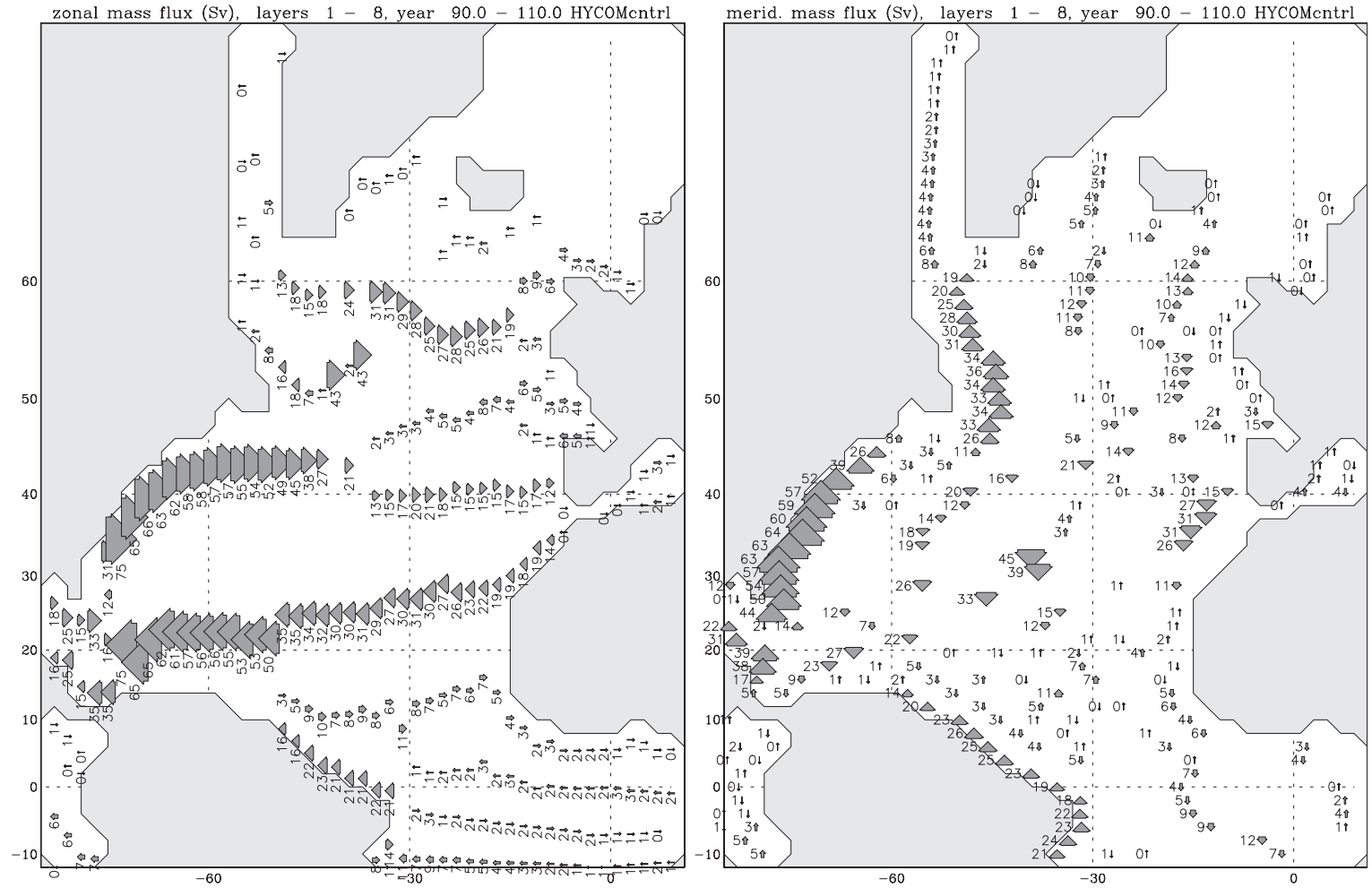


Fig. 6. Left: zonal component; right: meridional component of 20-year averaged mass flux in Atlantic basin, integrated both laterally and over isopycnic layers 1–8, for control run. Arrows indicate flux direction. Numbers written next to arrows indicate flux magnitude (Sv). See text for further details.

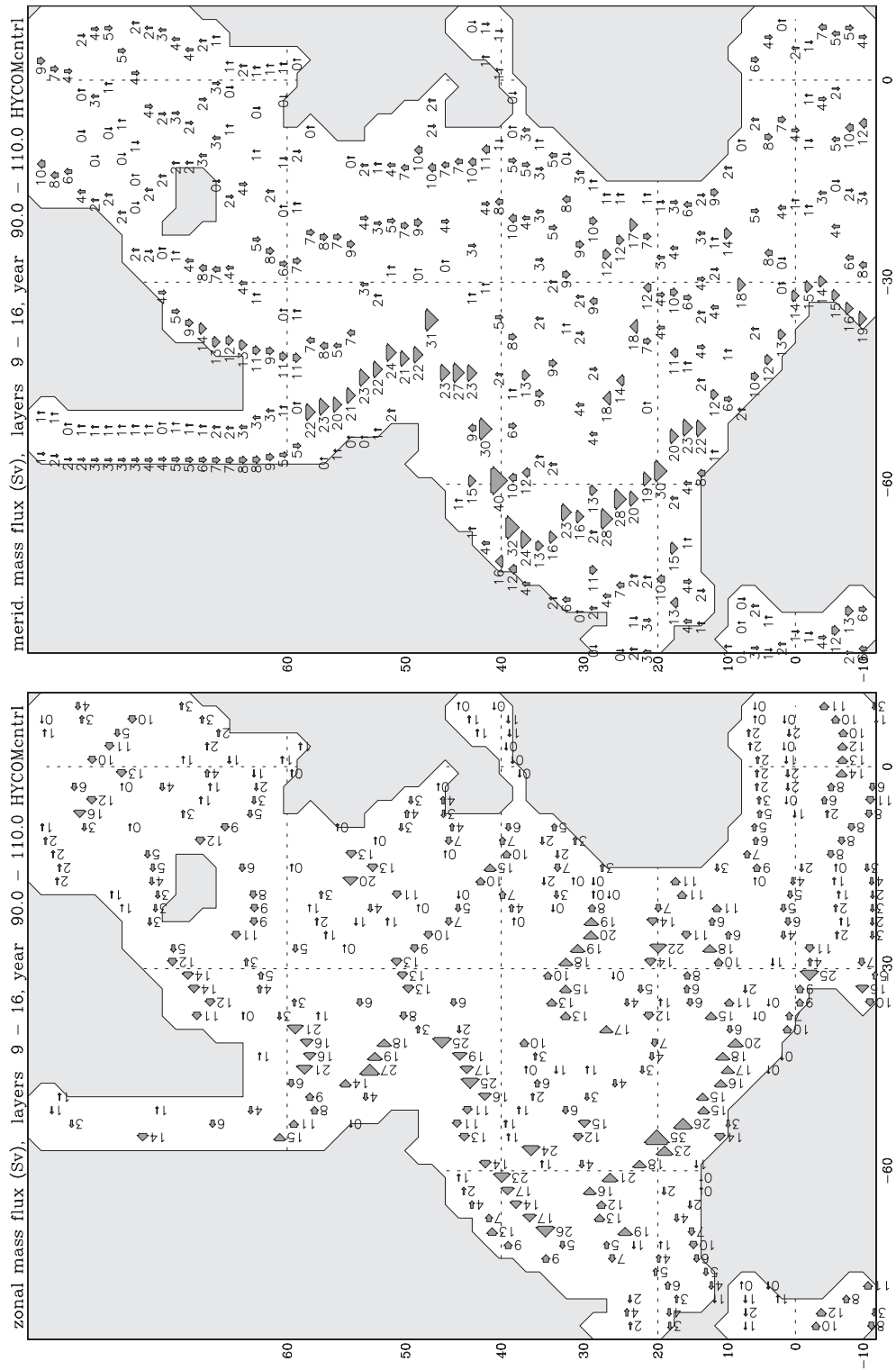


Fig. 7. As in Fig. 6, but for model layers 9–16.



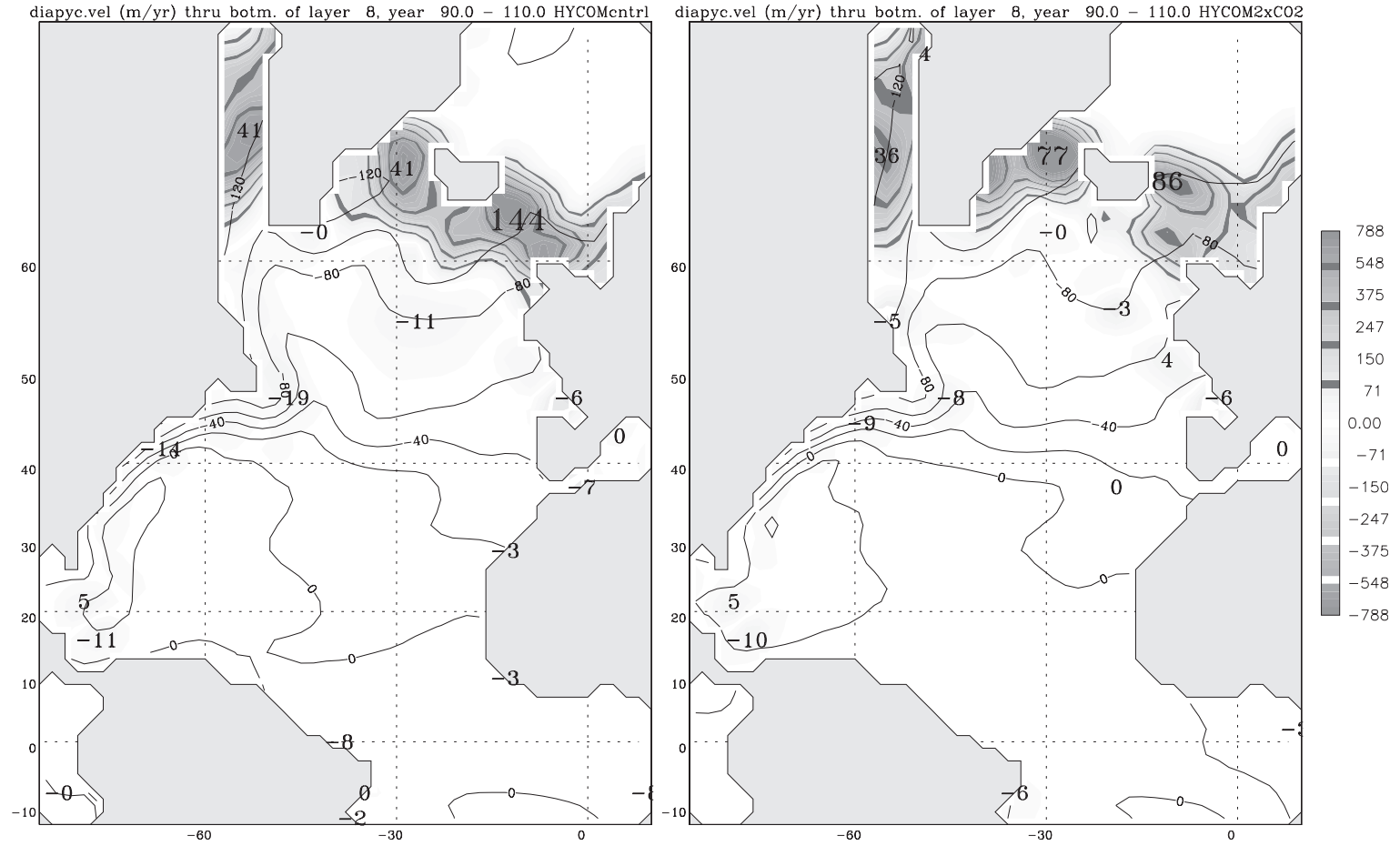


Fig. 8. Grey-shaded contours: 20-year averaged vertical motion ( $\text{m year}^{-1}$ , positive downward) through the interface separating isopycnic layers 8 and 9 ( $\sigma_2 = 36.61$  and  $36.79$   $\text{kg m}^{-3}$ ). Plain isolines: sea surface height (cm). Bold numbers: Total vertical transport (0.1 Sv) associated with individual patches of vertical motion. Left: control run. Right:  $2 \times \text{CO}_2$  run.

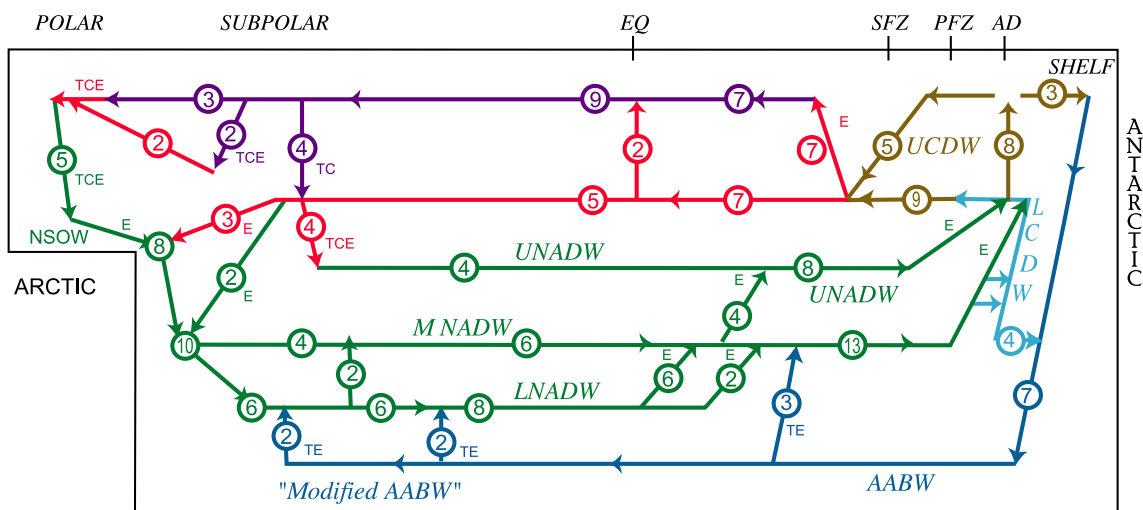


Fig. 9. A six-vertical layer section for the Meridional Overturning Circulation in the Atlantic Ocean, with a simplified global linkage involving Circumpolar Deep Water (CDW). Purple denotes an upper layer, red intermediate, green deep, and blue bottom water. Lower Circumpolar Deep Water (LCDW) is identified with light blue or cyan lines in the vicinity of the ACC, whereas Upper CDW is denoted there by the color brown. There are three branches (green) for NADW: Upper, Middle and Lower North Atlantic Deep Water (UNADW, MNADW, LNADW). AABW is Antarctic Bottom Water, EQ denotes the equator, SFZ is Subpolar Frontal Zone, PFZ is Polar Front Zone and AD is Antarctic Divergence. Transports in Sverdrups in circles. Reproduced from Schmitz (2002) with author's permission.

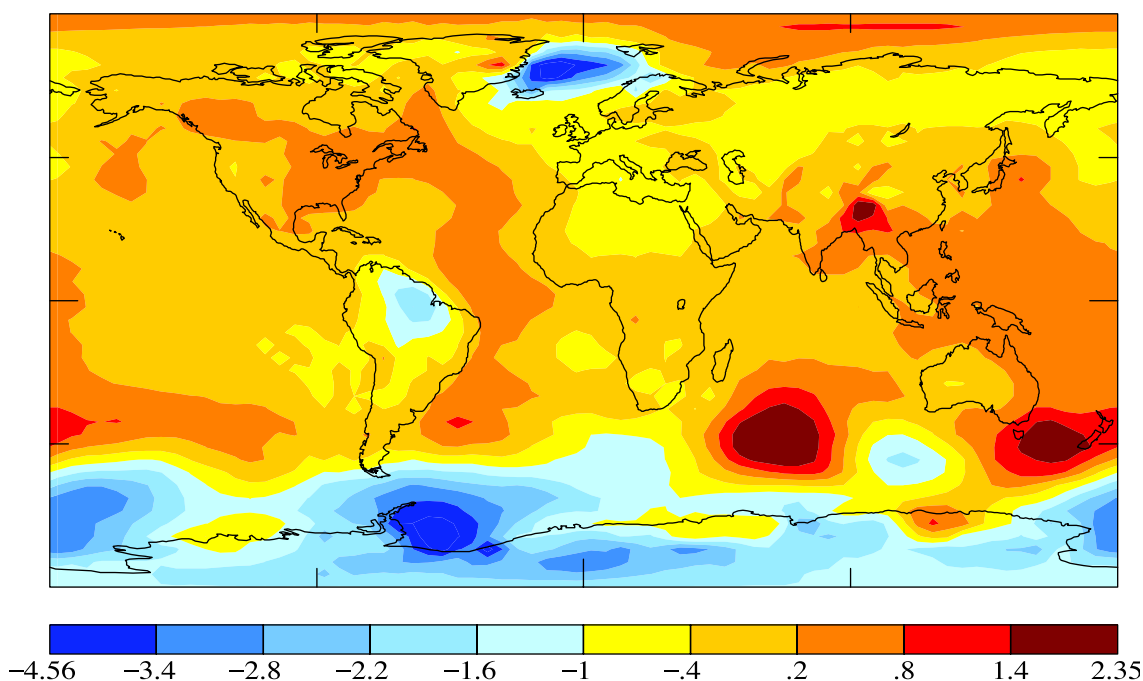


Fig. 10. Twenty-year average of sea level pressure difference (mb), CO<sub>2</sub> doubling minus control run.

find differences in the isopycnal mass fluxes that again are too small to warrant displaying them here.

In our suite of analysis products, the one involving the least amount of spatial averaging is the diapycnal flux field. Indeed, this field retains a few regional differences between the control and the CO<sub>2</sub> doubling run. Whereas the bulk of the downwelling in the control run takes place in the Norwegian Sea (left panel of Fig. 8), the Irminger and Norwegian Seas are shown in the right panel of Fig. 8 to be of comparable importance as downwelling sites in the CO<sub>2</sub> doubling run. We attribute this westward shift to the intensification of an atmospheric low-pressure area north of Iceland in the CO<sub>2</sub> doubling run, shown in Fig. 10. This low is associated with enhanced cold air advection west of Iceland and warm air advection east of

Iceland, making the Irminger Sea a more favorable place for deep water formation than it is in the control run.

Broadly speaking, the model tends to form the densest water in the immediate vicinity of the polar ice edge. The slight northward shift of the downwelling region in the Norwegian Sea seen in the right panel of Fig. 8 is an indication that the ice edge is predicted to retreat during global warming.

Because the model predicts greater ice loss around Antarctica than in the North Atlantic, the poleward shift of the zone of maximum downwelling during global warming is actually more pronounced in the southern hemisphere than in the North Atlantic. The two panels in Fig. 11 illustrate this shift. Given that the ice model used in these experiments is a purely

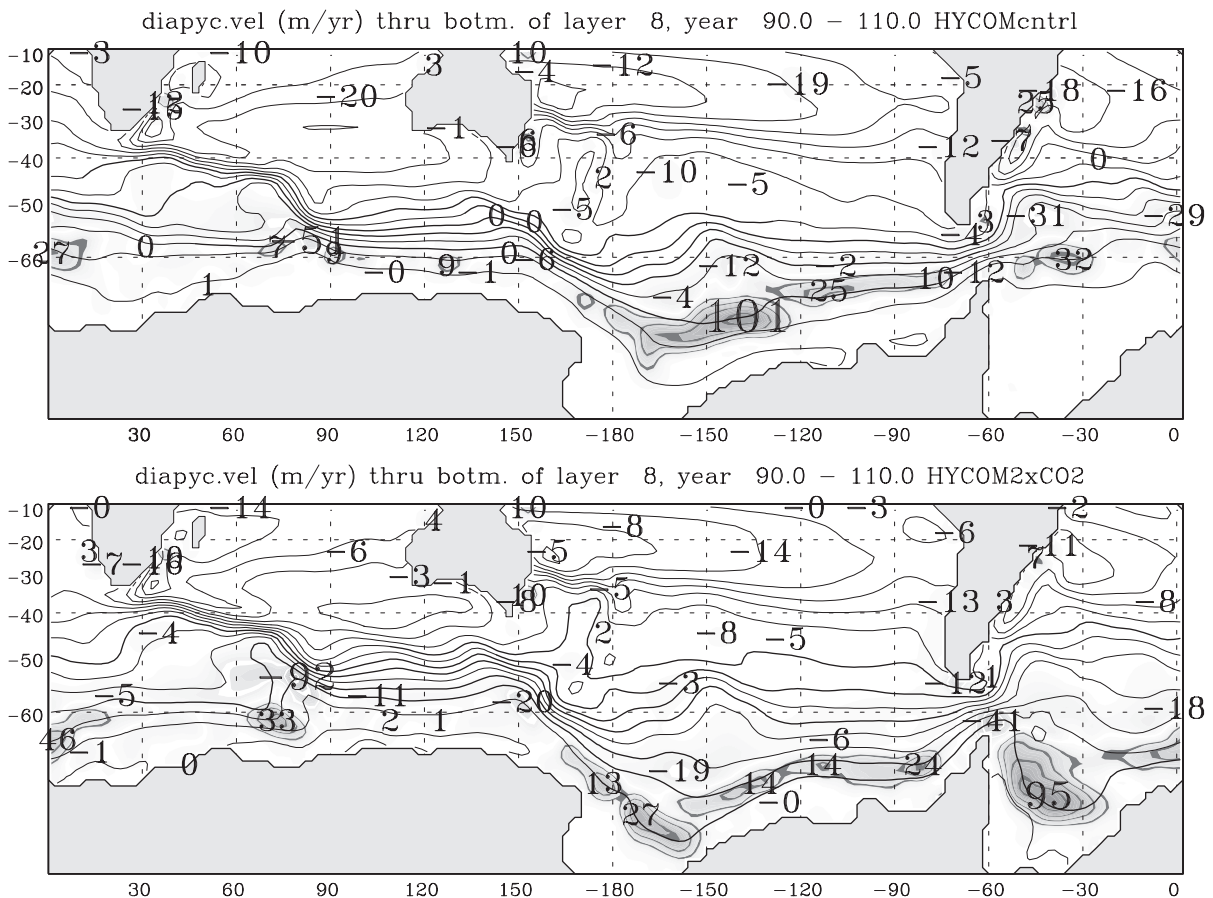


Fig. 11. Same as Fig. 8, except for the Southern Ocean.

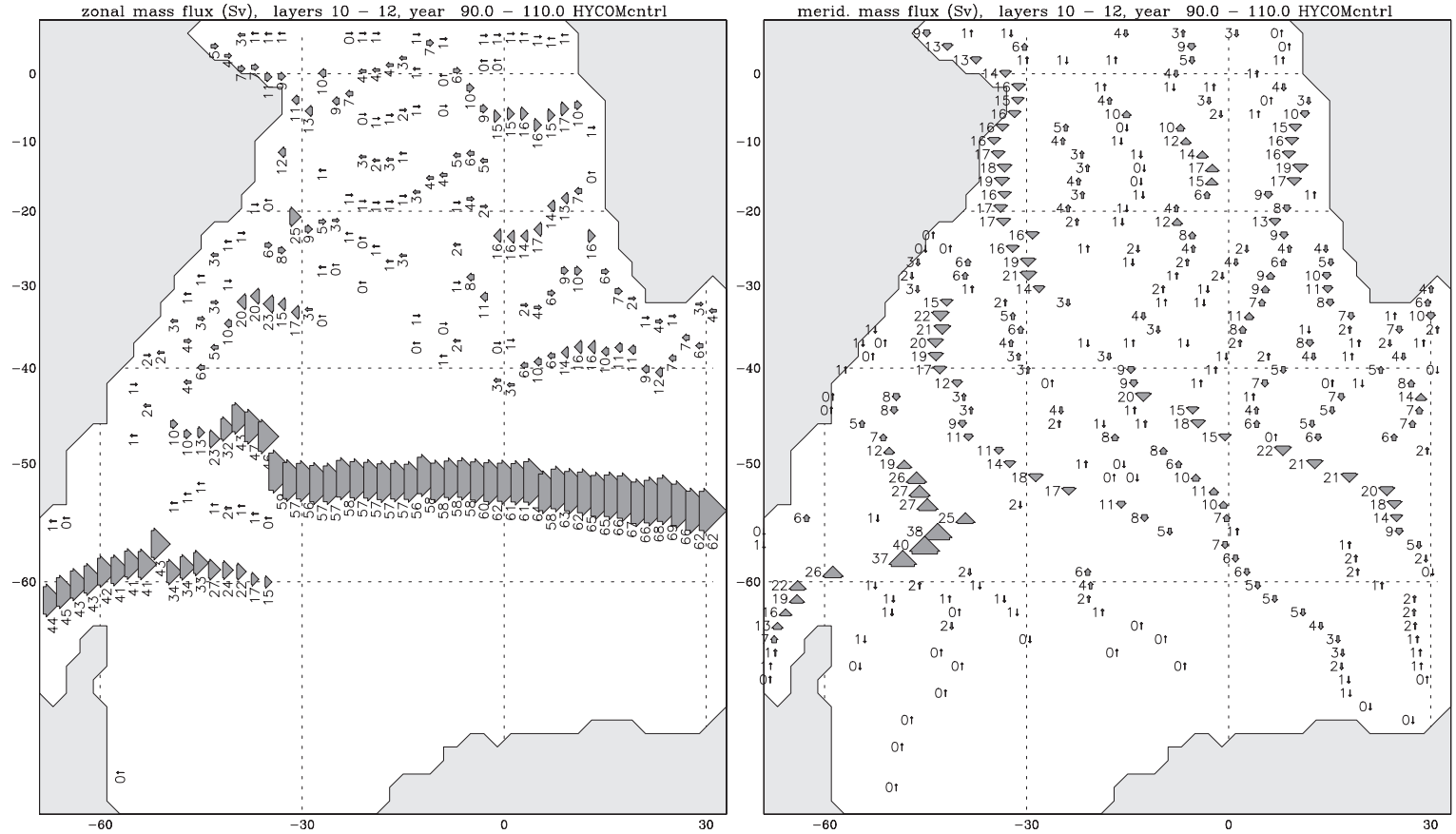


Fig. 12. Zonal and meridional mass fluxes in isopycnic layers 10–12 in the South Atlantic, control run. See Fig. 6 for other details.

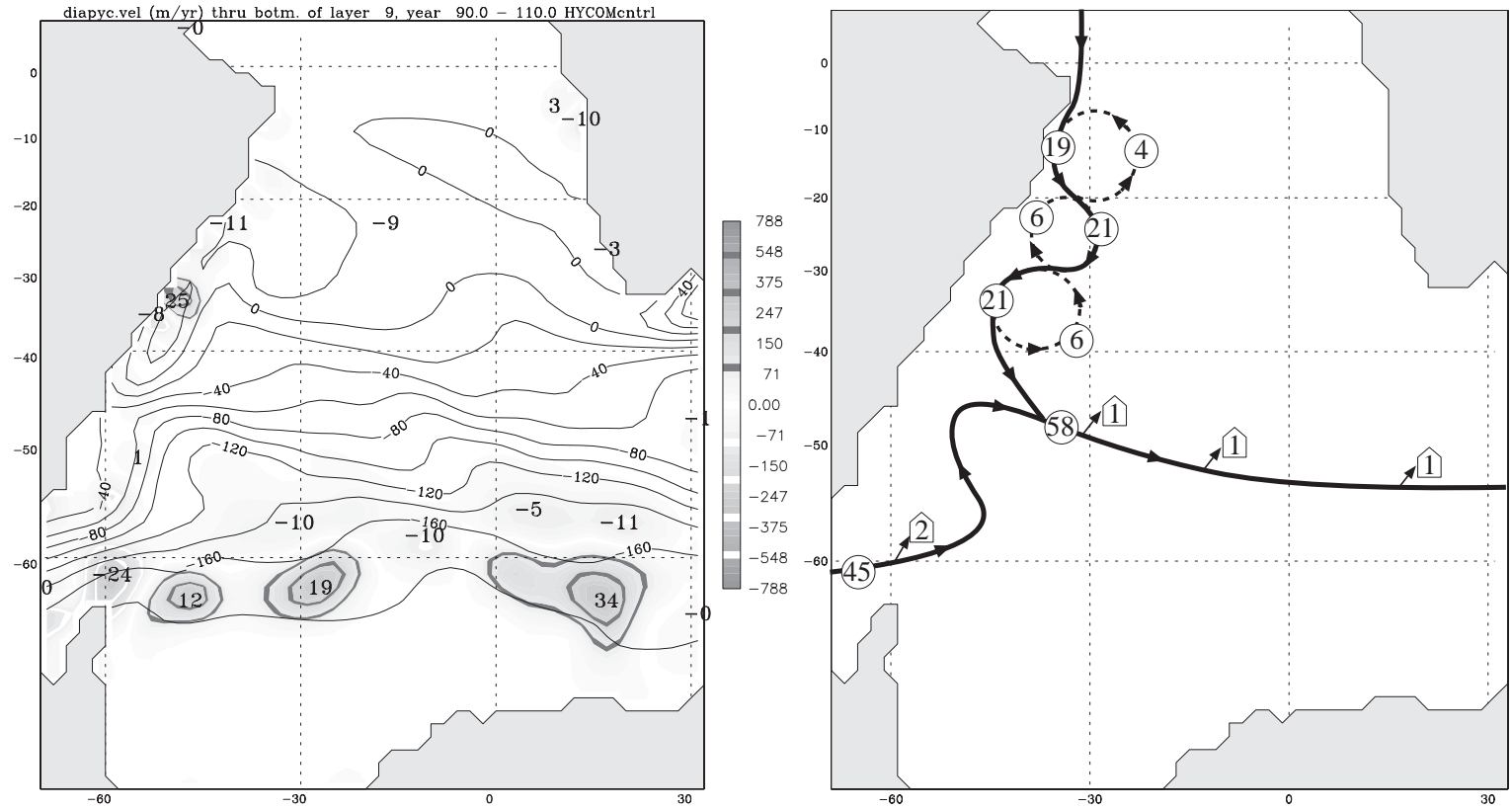


Fig. 13. Left: diapycnal mass fluxes through interface separating isopycnal layers 9 and 10 in control run; see Fig. 8 for other details. Right: Schematic of isopycnal mass fluxes within layers 10–12 (circled numbers, Sv) and upward diapycnal mass fluxes through the interface separating layers 9 and 10 (numbers in pentagons, Sv).

thermodynamic one, that is, does not incorporate ice transport or lateral spreading, the features depicted in Fig. 11 probably are of no quantitative significance. However, the appearance of the 9.5 Sv downwelling center in the Weddell Sea and the weakening of the 10.1 Sv downwelling center near 140°W in the CO<sub>2</sub> doubling run correlates well with the sea level pressure changes seen in Fig. 10. The prominent drop in surface pressure over the Weddell Sea creates stormy conditions, enhancing dense water production through evaporative freshwater loss (salinity increase), while the pressure rise east of the Ross Sea adds a warm-air advection component to the circulation there, suppressing dense water production to some extent.

In a widely discussed paper, Toggweiler and Samuels (1995) argue that wind-driven upwelling in the Southern Ocean plays an important role in maintaining the interhemispheric MOC cell in the Atlantic. Schmitz (2002) estimates the strength of the interhemispheric transport to be 18 Sv (see Fig. 9). In qualitative agreement with this notion, Hirst and McDougall (1998, Fig. 4), Marsh et al. (2000, Fig. 14a), and Speer et al. (2000, Fig. 4) all show streamlines connecting the northern sinking region to the wind-driven upwelling zone in the Antarctic Circumpolar Current (ACC). In contrast to this, panel (d) of Fig. 4 shows a remarkably symmetric double-cell structure for the MOC, even though panel (a) of Fig. 4 indicates that roughly 14 Sv of water in model layers 10–12 exit the Atlantic at the latitude of Cape of Good Hope. What happens to this water on its way south?

To shed light on this issue and again demonstrate the utility of our analysis method, we will track the southward flow of NADW water past the latitude of Cape of Good Hope in our model. To this end, we show in Fig. 12 the 20-year time averages of the isopycnal mass fluxes in layers 10–12 combined. The diapycnal flux through the interface separating layers 9 and 10, shown in the left panel of Fig. 13, reveals zones of upward motion north of the ACC axis and downward motion south of it, the former presumably associated with Ekman suction and the latter associated with the thermally driven downward limb of the southern overturning cell.

While the many recirculation cells seen in Fig. 12 paint a somewhat confusing picture of NADW water movement in the subtropical South Atlantic, closer

inspection reveals the presence of a strand of 15 Sv of water which, after crossing the equator near the Brazilian coast and passing through three recirculation gyres, merges with the ACC north of the Weddell Sea. The spatial organization of this movement is shown schematically in the right panel of Fig. 13. Once it merges with the ACC, this North Atlantic water loses its identity, and its subsequent fate cannot be determined solely from the Eulerian mass flux information which our analysis technique is based on. Nevertheless, the 15 Sv of NADW that we have confirmed as reaching the ACC must eventually return to the North Atlantic at lower density, as indicated in panel (a) of Fig. 4. Hence, water must upwell in the Southern Ocean at the rate of 15 Sv (a value commensurate, as it should, with Ekman theory). Given the proximity and patchiness of the up- and downwelling areas along the ACC, shown for the Atlantic sector in Fig. 13, it is not surprising that no upwelling streamlines are found in panel (d) of Fig. 4. Stated differently, zonal averaging creates a blend of wind-driven upwelling and buoyancy-driven sinking with the latter overshadowing the former.

## 5. Concluding remarks

We have demonstrated a technique for condensing output from an ocean model in a way that reveals coarse-grain geographic features of the 3-D buoyancy and wind-forced circulation in the model. Development of this technique has been inspired by analogous work in the observational oceanographic community. Emphasis here is on the thermohaline-forced vertical-meridional circulation which together with the atmosphere plays a leading role in redistributing heat on the planet. Tools like the one presented are important for investigating feedback mechanisms involving the ocean circulation in climate models. A detailed understanding of these mechanisms will help the research community distinguish climate fluctuations that are due to natural variability from changes caused by anthropogenic alterations of atmospheric composition.

Decomposing the 3-D circulation into its iso- and diapycnal components, and reducing it in the manner demonstrated here, is particularly easy if the ocean model itself is framed in isopycnal coordinates. How-



ever, experience gained at Los Alamos National Laboratory in comparing the MOC in two ocean models (MICOM and a traditional  $z$  coordinate model named POP) has shown that the requirement to transform  $z$  coordinate model fluxes to isopycnic space is no obstacle to displaying and analyzing output in the manner shown here. Readers intending to apply this technique to output from a  $z$  coordinate model should remain aware of the delicate balance of vertical and horizontal mass fluxes that is the trademark of hydrostatic models. Hence, it is paramount in such an analysis to start from horizontal mass fluxes which exactly match those used to solve the ocean model's continuity equation, and to transform them into density space in a manner that preserves their column integral. A coordinate transform scheme developed for this purpose (among others) is described in [Appendix D of Bleck \(2002\)](#).

The overarching climate dynamics question driving this work is whether the Atlantic MOC should, or should not, be expected to weaken under a  $\text{CO}_2$  doubling scenario. In the early coupled models, which used rather coarse meshes and perhaps were overly diffusive, the MOC was anything but a robust feature. Advances in modeling know-how and spatial resolution over the years have improved MOC stability, at least in models maintaining constant atmospheric greenhouse gas concentrations. Now that the MOC is stable in simulations of the present climate, the battle over the likely causes of its “volatility” in numerical models is being fought in the context of global warming experiments where static stability trends associated with surface warming and/or freshwater input may create new barriers for the MOC. It is too early to state with any degree of certainty whether the decline seen in most model simulations compiled in [Fig. 9.21 of IPCC \(2001\)](#) is due to numerical errors or reflects a legitimate response to changes in the atmospheric environment. Recent publications, such as [Sun and Bleck \(2001b\)](#) and others referenced therein, paint a picture which makes a strong decline of the Atlantic MOC during  $\text{CO}_2$  doubling appear less likely.

## Acknowledgements

The analysis tools illustrated here were originally developed under sponsorship of the Department of

Energy, Grant DE-FG02-98ER62608. The bulk of HYCOM development was funded by the Office of Naval Research under Grant No. N00014-97-1-0096. Research by RB is presently sponsored by the U.S. Department of Energy under the Climate Change Prediction Program. Research by SS is sponsored by NASA/Rutgers University Cooperative Agreement NCC5-476. Model runs were carried out at the Goddard Institute for Space Studies.

## References

- Arfken, G., 1970. *Mathematical Methods for Physicists*, 2nd ed. Academic Press, New York. 815 pp.
- Bleck, R., 2002. An oceanic general circulation model framed in hybrid isopycnic-Cartesian coordinates. *Ocean Model.* 4, 55–88.
- Hansen, J., et al., 1997. Forcings and chaos in interannual to decadal climate change. *J. Geophys. Res.* 102, 25679–25720.
- Hansen, J., et al., 2002. Climate forcings in Goddard Institute for Space Studies SI2000 simulations. *J. Geophys. Res.* 107 (D18), 4347 (doi: 10.1029/2001JD001143).
- Hirst, A.C., McDougall, T.J., 1998. Meridional overturning and diapycnal transport in a  $z$ -coordinate ocean model including eddy-induced advection. *J. Phys. Oceanogr.* 28, 1205–1223.
- IPCC, 2001. In: Houghton, J.T., et al., (Eds.), *Climate Change 2001: The Scientific Basis*. Cambridge Univ. Press, Cambridge. 881 pp.
- Levitus, S., Burgett, R., Boyer, T.P., 1994. NOAA world ocean atlas 1994. vol. 3 and 4, 99 and 177 pp. Natl. Oceanogr. Data Cen., Washington, DC.
- Macdonald, A.M., 1998. The global ocean circulation: a hydrographic estimate and regional analysis. *Prog. Oceanogr.* 41, 281–382.
- Marsh, R., Nurser, A.J.G., Megann, A.P., New, A.L., 2000. Water mass transformation in the Southern Ocean of a global isopycnal coordinate GCM. *J. Phys. Oceanogr.* 30, 1013–1045.
- Russell, R.L., Miller, J.R., Rind, D., Ruedy, R., Schmidt, G., Sheth, S., 2000. Comparison of model and observed regional temperature changes during the past 40 years. *J. Geophys. Res.* 105, 14891–14898.
- Schmitz Jr., W.J., 1996. On the World Ocean Circulation: Volume I. Some global features/North Atlantic Circulation. Woods Hole Oceanogr. Inst., Tech. Rep. WHOL-96-03.
- Schmitz Jr., W.J., 2002. On the circulation in and around the Gulf of Mexico—Volume I. A review of the deep water circulation, in preparation (draft at <http://www.cbi.tamucc.edu/~gomcirculation/> dated April 9, 2002).
- Speer, K., Guilyardi, E., Madec, G., 2000. Southern ocean transformation in a coupled model with and without eddy mass fluxes. *Tellus* 52A, 554–565.
- Sun, S., Bleck, R., 2001a. Thermohaline circulation studies with an isopycnic coordinate ocean model. *J. Phys. Oceanogr.* 31, 2761–2782.

- Sun, S., Bleck, R., 2001b. Atlantic thermohaline circulation and its response to increasing CO<sub>2</sub> in a coupled atmosphere–ocean model. *Geophys. Res. Lett.* 28, 4223–4226.
- Sun, S., Bleck, R., Rooth, C.G.H., Dukowicz, J., Chassignet, E.P., Killworth, P., 1999. Inclusion of thermobaricity in isopycnic-coordinate ocean models. *J. Phys. Oceanogr.* 29, 2719–2729.
- Toggweiler, J.R., Samuels, B., 1995. Effect of Drake Passage on the global thermohaline circulation. *Deep-Sea Res.* 42, 477–500.
- Trenberth, K.E., Caron, J.M., 2001. Estimates of meridional atmosphere and ocean heat transport. *J. Climate* 14, 3433–3443.